IIETA International Information and Engineering Technology Association
Advancing the World of Information and Engineering

Annales de Chimie - Science des Matériaux
Vol. 50, No. 1, February, 2025, pp. 99-105
Journal homepage: http://iieta.org/journals/acsm

Ag/MNO₂ Nanocomposites: Synthesis and Characterization Using Q-Switched Pulsed Nd-YAG Laser Ablation

Saif M. Alshrefi, Hassan A. Majeed, Mariam Kadhim Jawad, Ali Samer Mohammed, Donia Mohsen Diwan, Duaa Maged Ali, Mohammed Hamza K. AL-Mamoori*

Laser Physics Department, College of Science for Women, University of Babylon, Hilla 51001, Babylon, Iraq

Corresponding Author Email: Wsci.mohamed.hamza@uobabylon.edu.iq

https://doi.org/10.18280/acsm.500110

Received: 13 December 2025
Revised: 2 February 2026
Accepted: 12 February 2026
Available online: 28 February 2026

Keywords:
silver/manganese dioxide nanocomposites, laser ablation, removal of environmental pollutants

ABSTRACT

A Q-switched pulsed Nd: YAG laser ablation technique was used to synthesize the silver/manganese dioxide nanocomposites (AgNPs/MnO_2NPs), and their structural and optical characteristics were investigated. AgNPs and MnO_2NPs were separately synthesized by pulsed laser ablation in liquid (PLAL) and then combined to generate the Ag/MnO_2 nanocomposites. Ultraviolet-Visible (UV-Vis) spectroscopy was used to analyses the optical properties, which showed the surface plasmon resonance (SPR) peaks for AgNPs and the absorption edge for MnO_2NPs. After mixing AgNPs and MnO_2NPs, the absorption edge of AgNPs/MnO_2NPs showed a blue-shift compared to MnO_2NPs and AgNPs, the associated energy band gap of MnO_2NPs and AgNPs/MnO_2NPs were 3.5 eV and 4.0 eV, respectively. Green luminescent emission (PL) from MnO_2 (~550 nm), which correlated to defect-related emissions and AgNPs emissions. The crystallinity, size distribution and morphology of the nanoparticles were confirmed by X-ray diffraction (XRD) and scanning electron microscopy (SEM). These findings indicate that the optical performance of the AgNPs/MnO_2 nanocomposites is improved, resulting from the synergism between AgNPs and MnO_2NPs, and suggest that the nanocomposites may be potential optical devices, sensors and photocatalyst novel candidate materials.

1. INTRODUCTION

Particularly in optoelectronics, catalysis, and biomedical applications, nanocomposite materials have attracted a lot of interest and are quite valuable due to their unique optical and structural properties [1, 2]. Whereas silver nanoparticles (Ag NPs) have an antimicrobial activity, high electrical conductivity, and strong surface plasmon resonance (SPR) [3], MnO_2 is well-known for its vast surface area, tunable bandgap, and catalytic effectiveness [4, 5]. When coupled with Ag NPs), a material known for its magnetic and catalytic properties, the resulting Ag/MnO nanocomposites are expected to demonstrate synergistic effects. Better structural and optical characteristics can follow from this. Among the several preparation techniques, the laser ablation method distinguishes itself since it generates high-purity nanomaterials with exactly regulated size, shape, and content [6]. This method is quite helpful for producing nanocomposites with unique structural and optical features since the laser parameters can be adjusted to fine-tune the material properties. This work synthesized MnO_2 nanoparticles following Ag NPs originally produced by pulsed laser ablation in liquid (PLAL) [7], MnO_2 nanoparticle manufacturing comes next. Ag/MnO_2 nanocomposites were produced by combining the two components and then investigated structurally and optically using a variety of techniques. We investigated Ag/MnO_2 nanocomposites [8] in optical terms using a Ultraviolet-Visible (UV-Vis) spectrophotometer. The outcomes of this work expand our understanding of Ag/MnO nanocomposites and show the need of exact control over material synthesis techniques such as laser ablation for the future development of complex optical devices and sensors.

2. EXPERIMENTAL PART

The samples' morphology was examined by a JSM-6510LV field emission scanning electron microscopy (FESEM) Type - S-1640 HITACHI business Japan under reflection geometry with a Shimadzu 6000 X-ray diffractometer (built in JAPAN), the sample structure was investigated using (Cu Kα) radiation (λ = 1.5406 Å). Mid-IR spectra from (4000 - 400 cm^{-1}) were collected using Fourier Transform Infrared Spectroscopy (FTIR)-Spectrometer, supplied by ALPHA (Made in Germany), for some pure materials and all doped samples. To estimate the spectra for FTIR, Potassium Bromide (KBr) powder was blended with powder samples. The optical characteristics (CECIL CE 7200, ENGLAND) of every produced material were obtained using a UV-Vis diffused reflectance spectroscope.

2.1 Preparation of nanocomposites

Laser ablation method was used in silver/manganese dioxide nanocomposites (AgNPs/MnO_2NPs). Target immersion for pure silver (Ag) and MnO_2 NPs was separately in 10 mL of distilled water. Target Ag and MnO_2 was ablated using Q-Switched a Nd: YAG pulsed laser (wavelength 1064 nm, 3 Hz, 300mj and 300 pulses). This is depicted in Figure 1. The surface of Ag and MnO_2 target was the focus of the laser beam, which produced suspended Ag and MnO_2 nanoparticles correspondingly; subsequently, their optical and structural characteristics are determined. Mixed a colloidal solution of AgNPs with MnO_2 NPs in a 1:1 volume ratio as described in flowchart to synthesize Ag/MnO_2 nanocomposites.

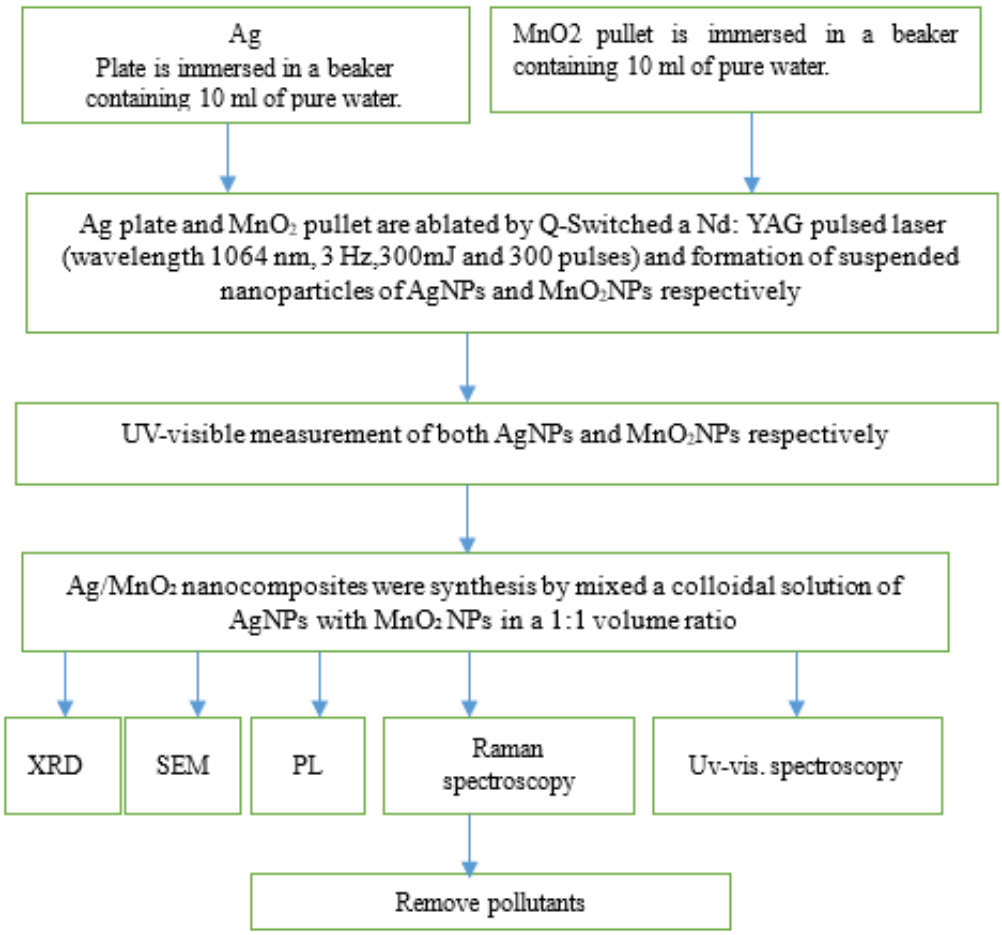

Figure 1. Flowchart for the synthesis of Ag/MnO_2 nanocomposite

3. RESULTS AND DISCUSSION

3.1 Optical properties

Consistent with what is reported in the reference [9-11], the peak at 403.4 nm denotes the resonance frequency of the electron oscillations of AgNPs as shown in Figure 2. The energy gap was calculated from the blank equation Eg (eV) = 1240/λ(nm) andis equal to 3.07 eV.

The MnO_2NPs' absorption spectra consistent with what is reported in the reference [12, 13], revealing a typical absorption edge in the UV range at 326.5 nm as shown in Figure 3. The significant UV absorption and relative transparency in the visible range arising from the quantum confinement phenomenon occurring from the employment of pulsed laser and this promises to be used in UV filtering, photocatalyzed, optical sensing.

The absorption spectrum of the Ag/MnO_2 nanocomposite shows the presence of an absorption edge at 300 nm as shown in Figure 4. A blue shift is observed for the absorption edge of the MnO_2NPs particles in the Ag/MnO_2 nanocomposite because of Quantum confinement effects or interactions between MnO_2NPs and AgNPs in nanocomposite. Combining MnO_2 nanoparticles with AgNPs causes changes in the electrical structure of MnO_2 such that the absorption edge of MnO_2 moves to somewhat shorter wavelengths (blue shift) and this behavior is similar to what was stated in the reference [14].

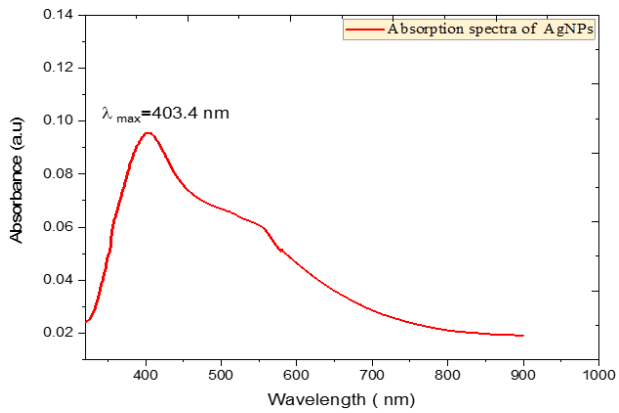

Figure 2. Absorption spectra of AgNPs (Surface Plasmon Resonance)

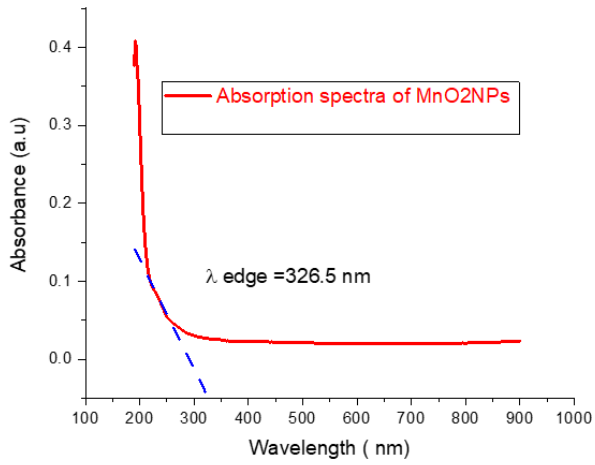

Figure 3. Absorption spectra of MnO_2 nanoparticles

The energy gap of the MnO_2NPs and Ag / MnO_2 nanocomposite was calculated using the Tuck-Plot equation as shown in Figures 5 (a) and (b) and was equal to 3.5 eV and 4 eV for MnO_2NPs and Ag/MnO nanocomposite respectively. Tauck Plot equation deal with connection between the photon energy (hυ) and the absorption coefficient (α) as in $\alpha h\upsilon = A(h\upsilon - E_g)^n$) where (h) is the plank constant; (ϋ) is photon frequency; (hυ) is photon energy in eV; (Eg) is optical band gap in eV; (A) is a constant; (n) is an exponent whose value is (2) for indirect band transitions and (1/2) for direct band transition and (α) is the absorption coefficient as mentioned in the reference [15]. The intercept provides the transition band gap when the straight section of the graph of (αhv)2 against (hυ) is extrapolated to (α = 0).

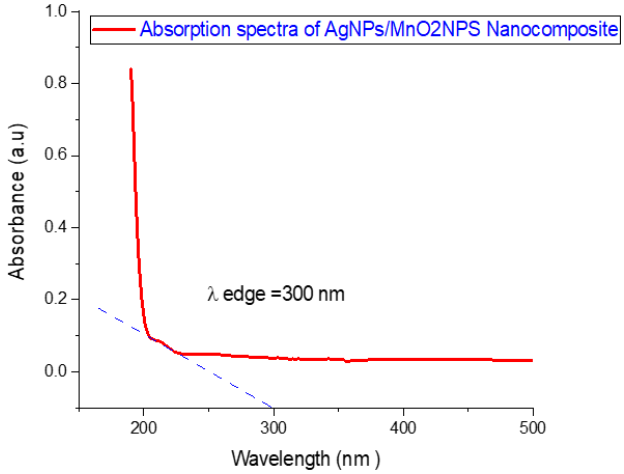

Figure 4. Absorption spectra of Ag/MnO_2 nanocomposite

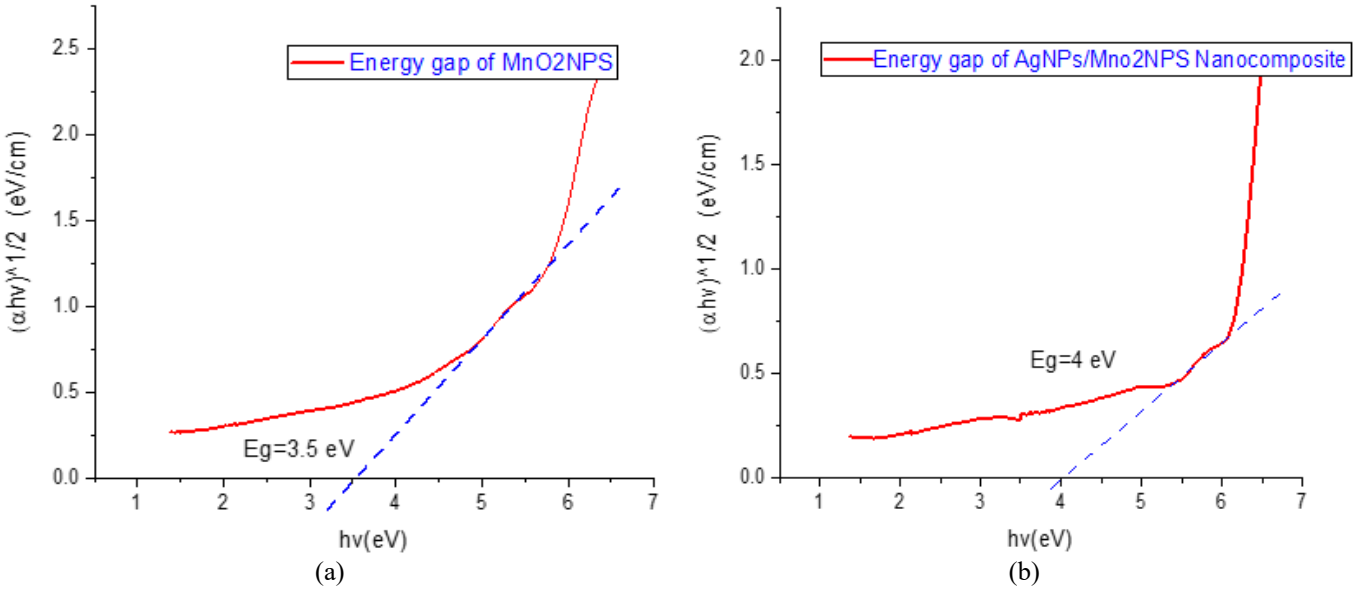

Figure 5. Energy gap of (a) MnO_2 nanoparticles and (b) Ag/MnO_2 nanocomposite

The quantum confinement affects that increase the band gap with smaller particle size, charge transfer and hybridization of electronic states between AgNPs and MnO_2 NPs, surface effects and strain at the interface between the two materials and modification of the MnO_2 band gap due of the interaction with AgNPs and this behavior is similar to what was stated in the references [14, 16, 17] and it's clear that the energy gap of the Ag / MnO_2 nanocomposite larger than the band gap of individual AgNPs or MnO_2 NPs and this is evidence of the smallness of the nanoparticles in the nanocomposite compared to the AgNPs and MnO_2 NPs alone.

3.2 Photoluminescence testing of Ag/MnO_2 nanocomposite

The PL emission of Ag/MnO_2 nanocomposite exhibit green luminescence at 554.6 nm as shown in Figure 6, which they ascribe to defect-related emission modes in the MnO_2 matrix and it is close to what was mentioned in the reference [18]. AgNPs added into MnO_2NPs can either strengthen or change the emission peaks. Because of interactions like SPR and charge transfer processes [19, 20], silver nanoparticles can particularly produce a blue shift or red shift in the PL spectrum.

Ag/MnO_2 nanocomposite Raman spectra are shown in Figure 7. A large peak cantered on 3442.9 cm^{-1} dominates. O-H stretching vibrations from adsorbed water or hydroxyl groups on the surface of the nanocomposite most certainly cause this. Combining AgNPs and MnO_2NPs in a nanocomposite allows the Raman spectra from the two materials to interact or overlap. The interactions among the

elements of the nanocomposite can produce either broadening, shifting, or suppression of particular Raman signals. Overlapping with other peaks, such as water or amplified scattering signals from other molecules, may hide or reduce the Raman peaks from AgNPs and MnO_2NPs. The large peak seen in your spectrum around 3442.9 cm^{-1} most likely results from O-H stretching from water or hydroxyl groups, easily masking smaller signals from AgNPs or MnO_2 [21, 22].

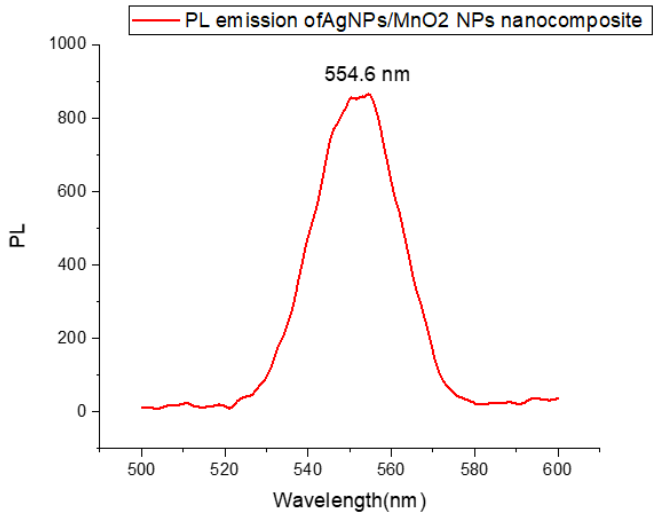

Figure 6. Photoluminescence (PL) emission spectra of Ag/MnO_2 nanocomposite

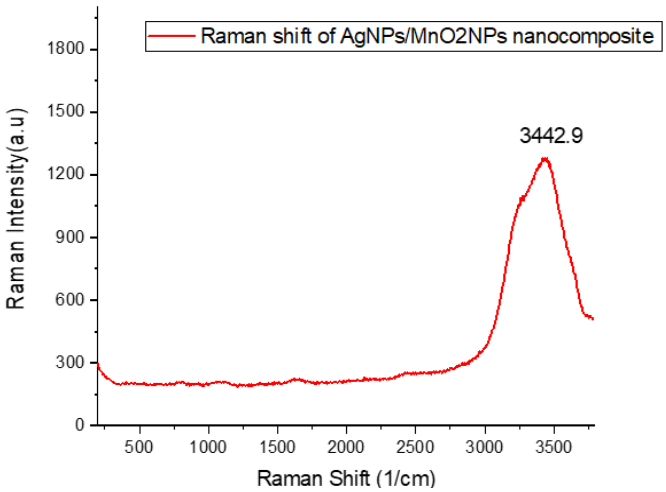

Figure 7. Raman spectrum of Ag/MnO_2 nanocomposite

3.3 X-Ray diffraction measurements

Layered/birnessite-type MnO_2 (low-angle (00l) basal reflections) are consistent with peaks at 2θ = 17.1° and 2θ = 14.1°; Joint Committee on Powder Diffraction Standards (JCPDS) birnessite patterns reveal first reflections in ~12–18°, as illustrated in Figure 8. These are not Ag metallic peaks (Ag major lines lie outside your 8–28° scan and occur at ≈ 38.1°, 44.3°, and 64.4° for Cu Kα). For MnO_2NPs, the crystallite size was determined using the Scherrer equation for peaks 14.10 and 17.10, which correspond to 1.4 nm and 1.6 nm, respectively. While Ag peaks are outside the scan range, the pattern mostly shows the presence of weakly crystalline MnO_2 layers. The peaks of the very small or poorly crystalline Ag nanoparticles created by the pulsed-laser approach broadened and weakened below detection.

3.4 Scanning Electron Microscopy of the prepared Ag/MnO_2 nanocomposite

The surface morphology of the Ag/MnO_2 nanocomposite produced by pulsed laser ablation is displayed in this SEM image. The MnO_2 matrix appears as a rough and porous background, and the bright spherical particles are Ag nanoparticles evenly distributed on it. As seen in Figures 9 (a-c), the image demonstrates the successful decoration of MnO_2 by Ag by the laser ablation process, confirming well-distributed nanosized Ag particles and high surface coverage.

The SEM image demonstrate a dual-morphology, with an ultrafine porous nanostructure (≈ 50 nm features) serving as the substrate and ornamented with larger, distributed nanoparticles and micro-aggregates, as seen in Figure 9 (d). This could be utilized to increase charge/discharge rates in energy storage devices (such as supercapacitors and batteries), as well as catalysis and antibacterial applications.

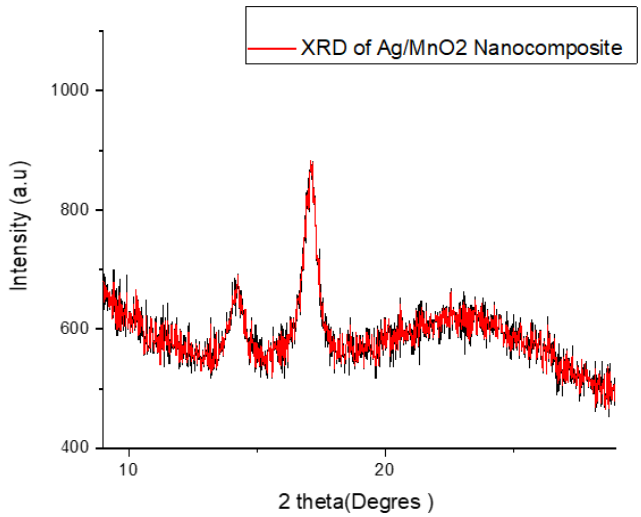

Figure 8. X-ray diffraction (XRD) measurements of Ag/MnO_2 nanocomposite

3.5 Using Ag/MnO_2 nanocomposite to remove methylene blue dye under the influence of a light source for different times

Ag/MnO_2 composite degradation of methylene blue (MB) dye is a high-efficiency technique based on advanced oxidation processes (AOPs) and synergistic photocatalysis, which is essential for contemporary wastewater treatment as shown in Figure 10, where MnO_2 functions as a potent oxidant and a catalyst for AOPs. It concentrates the dye close to the active sites due to its large surface area for MB molecule adsorption. Crucially, when oxidants (such H_2O_2) are activated, MnO_2 promotes the production of highly reactive oxygen species (ROS) like hydroxyl radicals ($\cdot OH$), which causes the dye to degrade quickly chemically. Ag's primary function is to increase photocatalytic efficiency when exposed to light. Ag nanoparticles draw photogenerated electrons from MnO_2 by acting as electron traps. This prolongs the lifetime of the charge carriers and increases the generation of ROS by suppressing the recombination of the electron-hole (e^-/h^+) pairs. Additionally, Ag demonstrates Localized Surface Plasmon Resonance (LSPR), which enables the catalyst to efficiently use solar energy and absorb more visible light. This behavior is comparable to that described in the references [23-25].

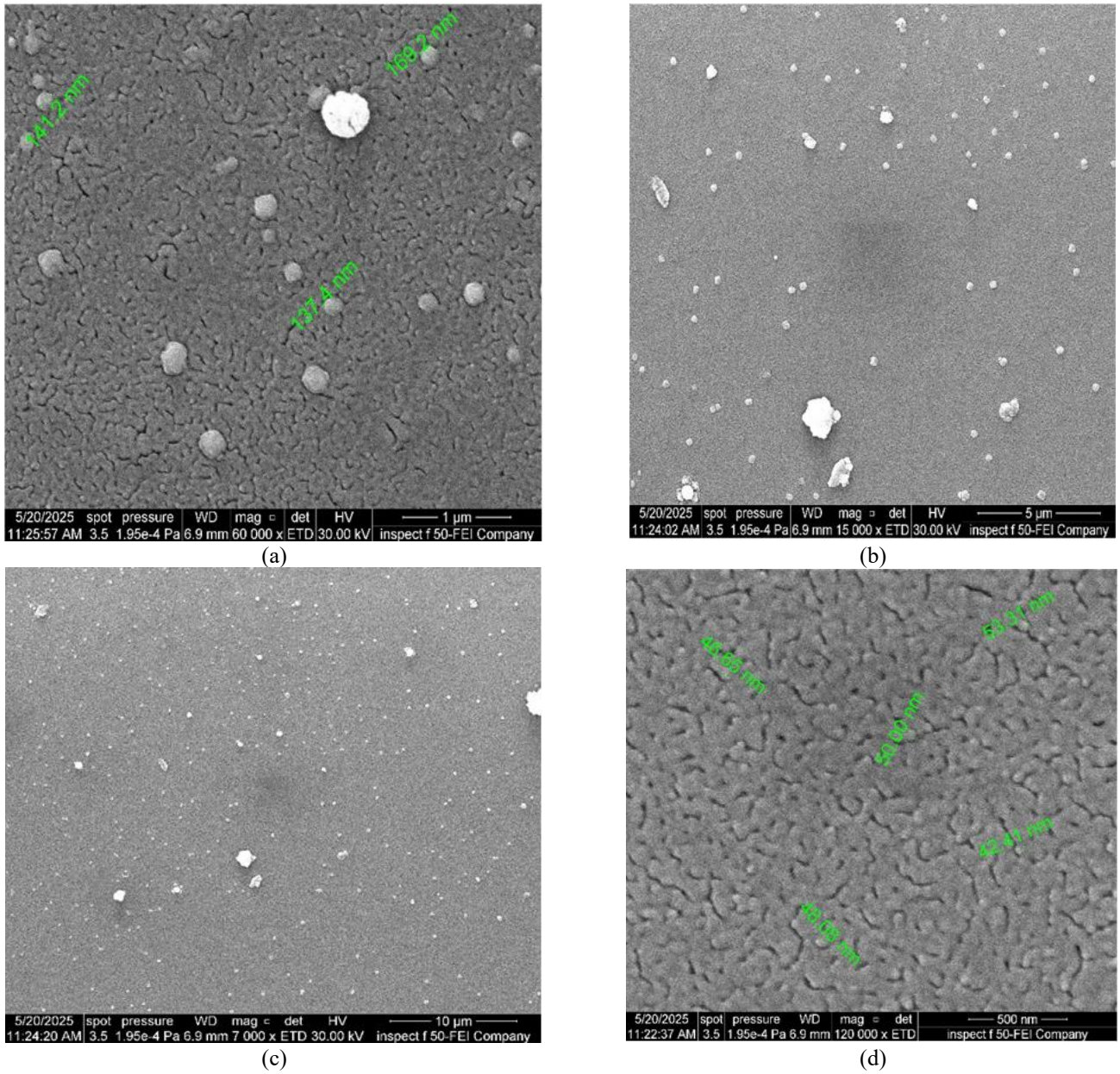

Figure 9. Scanning electron microscopy (SEM) images of Ag/MnO_2 nanocomposite (a) 1 micro, (b) 5 micros, (c) 10 micros, (d) 500 nm

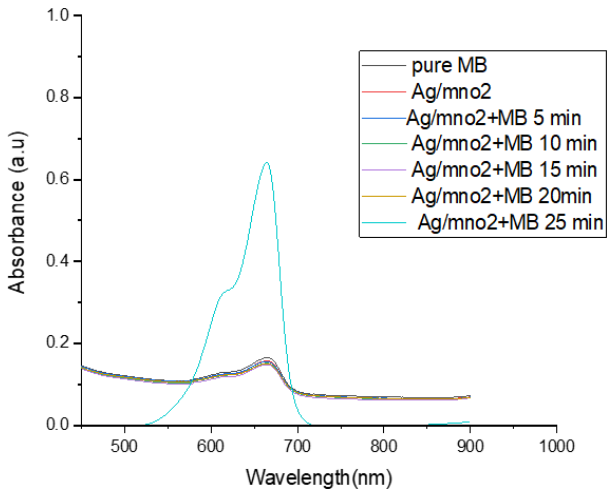

Figure 10. Photodegradation of methylene blue (MB) by the prepared Ag/MnO_2 nanocomposite for different times

4. CONCLUSION

This work effectively synthesized AgNPs/MnO_2NPs nanocomposites by Q-switched pulsed Nd: YAG laser ablation. The blue shift in the absorption spectrum shown by UV-Vis. spectroscopy indicated interaction between AgNPs and MnO_2NPs resulting in quantum confinement and modifications in the electronic structure. We calculated the nanocomposite's energy gap to be 4.0 eV. Green luminescence associated with MnO_2 shown by photoluminescence (PL) studies showed possible influence from AgNPs on flaws in MnO_2. XRD and SEM verified the crystalline character, size distribution (15-80 nm), and shape of the nanoparticles. The work emphasizes how synergistic interaction between AgNPs and MnO_2NPs results in enhanced optical characteristics of Ag/MnO_2 nanocomposites. With the laser ablation approach offering a consistent means for manufacturing high-quality nanocomposites with customizable properties, these nanocomposites are promising for uses like photocatalysis, sensors, and optical devices. A discernible change in charge

carrier dynamics upon Ag inclusion is indicated by the shift in the absorption edge and the associated change in PL emission intensity. Furthermore, the agreement between optical and structural analyses verifies that the observed changes in properties are directly related to the development of nanocomposites rather than experimental variability.

REFERENCES

[1] Baishya, G., Parasar, B., Limboo, M., Kumar, R., et al. (2024). Advancements in nanocomposite hydrogels: A comprehensive review of biomedical applications. Discover Materials, 4(1): 40. https://doi.org/10.1007/s43939-024-00111-8

[2] Werdehausen, D. (2021). Nanocomposites as Next-Generation Optical Materials. Springer International Publishing. https://doi.org/10.1007/978-3-030-75684-0

[3] Corrales, J., Acosta, J., Castro, S., Riascos, H., Serna-Galvis, E., Torres-Palma, R.A., Ávila-Torres, Y. (2022). Manganese dioxide nanoparticles prepared by laser ablation as materials with interesting electronic, electrochemical, and disinfecting properties in both colloidal suspensions and deposited on fluorine-doped tin oxide. Nanomaterials, 12(22): 4061. https://doi.org/10.3390/nano12224061

[4] Han, T., Xie, C.M., Meng, Y.J., Wei, Y. (2018). Synthesized MnO_2/Ag/g-C_3N_4 composite for photoreduction of carbon dioxide under visible light. Journal of Materials Science: Materials in Electronics, 29(24): 20984-20990. https://doi.org/10.1007/s10854-018-0243-2

[5] Wang, C., Bongard, H.J., Weidenthaler, C., Wu, Y., Schüth, F. (2022). Design and application of a high-surface-area mesoporous δ-MnO2 electrocatalyst for biomass oxidative valorization. Chemistry of Materials, 34(7): 3123-3132.

[6] Kim, M., Osone, S., Kim, T., Higashi, H., Seto, T. (2017). Synthesis of nanoparticles by laser ablation: A review. KONA Powder and Particle Journal, 34: 80-90. https://doi.org/10.14356/kona.2017009

[7] Baig, N., Kammakakam, I., Falath, W. (2021). Nanomaterials: A review of synthesis methods, properties, recent progress, and challenges. Materials advances, 2(6): 1821-1871. https://doi.org/10.1039/D0MA00807A

[8] Singh, N.B., Agarwal, S. (2016). Nanocomposites: An overview. Emerging Materials Research, 5(1): 5-43. https://doi.org/10.1680/jemmr.15.00025

[9] Razavi, R., Amiri, M., Alshamsi, H.A., Eslaminejad, T., Salavati-Niasari, M. (2021). Green synthesis of Ag nanoparticles in oil-in-water nano-emulsion and evaluation of their antibacterial and cytotoxic properties as well as molecular docking. Arabian Journal of Chemistry, 14(9): 103323. https://doi.org/10.1016/j.arabjc.2021.103323

[10] Widatalla, H.A., Yassin, L.F., Alrasheid, A.A., Ahmed, S.A.R., Widdatallah, M.O., Eltilib, S.H., Mohamed, A.A. (2022). Green synthesis of silver nanoparticles using green tea leaf extract, characterization and evaluation of antimicrobial activity. Nanoscale Advances, 4(3): 911-915.

[11] Jangid, H., Singh, S., Kashyap, P., Singh, A., Kumar, G. (2024). Advancing biomedical applications: An in-depth analysis of silver nanoparticles in antimicrobial, anticancer, and wound healing roles. Frontiers in Pharmacology, 15: 1438227. https://doi.org/10.3389/fphar.2024.1438227

[12] Al-Nidawi, A.J.A., Matori, K.A., Zakaria, A., Zaid, M.H.M. (2017). Effect of MnO_2 doped on physical, structure and optical properties of zinc silicate glasses from waste rice husk ash. Results in Physics, 7: 955-961. https://doi.org/10.1016/j.rinp.2017.02.020

[13] Meng, Y., Song, W., Huang, H., Ren, Z., Chen, S.Y., Suib, S.L. (2014). Structure–property relationship of bifunctional MnO2 nanostructures: highly efficient, ultra-stable electrochemical water oxidation and oxygen reduction reaction catalysts identified in alkaline media. Journal of the American Chemical Society, 136(32): 11452-11464. https://doi.org/10.1021/ja505186m

[14] Alalawi, A., Romman, U.E., Katubi, K.M., tul Shafa, S., et al. (2024). Ag-doped MnO_2 nanowires integrated with graphitic carbon nitride for enhanced photocatalytic applications for waste water treatment. Current Applied Physics, 60: 32-42. https://doi.org/10.1016/j.cap.2024.01.009

[15] Tran, T.T., Wong-Leung, J., Smillie, L.A., Hallén, A., Grimaldi, M.G., Williams, J.S. (2023). High hole mobility and non-localized states in amorphous germanium. APL Materials, 11(4): 041115. https://doi.org/10.1063/5.0146424

[16] Elbasuney, S., El-Khawaga, A.M., Elsayed, M.A., Elsaidy, A., Yehia, M., Correa-Duarte, M.A. (2024). Facile synthesis of silver doped manganese oxide nanocomposite with superior photocatalytic and antimicrobial activity under visible spectrum. Scientific Reports, 14(1): 15658. https://doi.org/10.1038/s41598-024-65749-z

[17] Derkaoui, K., Bencherifa, I., Hadjersi, T., Belkhettab, I., Bouanik, S., Brik, A., Kechouane, M., Kaci, M.M. (2024). MnO_2 decorated silicon nanowires: A novel photocatalyst for improved Rhodamine B removal under visible light exposure. Surfaces and Interfaces, 53: 105086. https://doi.org/10.1016/j.surfin.2024.105086

[18] Anguraj, G., Ashok Kumar, R., Inmozhi, C., Uthrakumar, R., Elshikh, M.S., Almutairi, S.M., Kaviyarasu, K. (2023). MnO_2 doped with Ag nanoparticles and their applications in antimicrobial and photocatalytic reactions. Catalysts, 13(2): 397. https://doi.org/10.3390/catal13020397

[19] Khan, Z., Al-Thabaiti, S.A. (2023). Photogenic MnO_2/Ag metal nanocomposites and their dye adsorbing activities. Journal of Saudi Chemical Society, 27(3): 101646. https://doi.org/10.1016/j.jscs.2023.101646

[20] Magesh, G., Arun, A.P., Poonguzhali, R.V., Kumar, E.R., Pradeep, I., Kumar, R.R., Abd El-Rehim, A.F. (2025). Pure α-MnO_2 and Ag decorated α-MnO2 nanorods for photocatalytic activity. Journal of Molecular Structure, 1329, 141444. https://doi.org/10.1016/j.molstruc.2025.141444

[21] Al-Thubaiti, K.S., Khan, Z., Al-Thabaiti, S.A. (2022). Effects of CTAB and SDS on the nucleation and growth of MnO2 and Ag-doped MnO2 nanoparticles formation. Journal of Molecular Liquids, 355: 118910. https://doi.org/10.1016/j.molliq.2022.118910

[22] Saravanan, R., Khan, M.M., Gupta, V.K., Mosquera, E., Gracia, F., Narayanan, V., Stephen, A.J.R.A. (2015). ZnO/Ag/Mn2O3 nanocomposite for visible light-

induced industrial textile effluent degradation, uric acid and ascorbic acid sensing and antimicrobial activity. RSC advances, 5(44): 34645-34651.

[23] Saeed, G., HK AL-Mamoori, M., N Madluim, K. (2023). Study of the optical, structural and adsorption properties of tellurium oxide nanoparticles and graphene nanosheets prepared by Q-switched Nd-YAG pulsed laser. Journal of Nanostructures, 13(3): 889-897. https://doi.org/10.22052/JNS.2023.03.030

[24] Aziz, H.M., Al-Mamoori, M.H., Aboud, L.H. (2021). Synthesis and characterization of TiO2-RGO nanocomposite by pulsed laser ablation in liquid (PLAL-method). Journal of Physics: Conference Series, 1818(1): 012206. https://doi.org/10.1088/1742-6596/1818/1/012206

[25] Al-Nafiey, A., Al-Mamoori, M.H., Shakir, A.K., Alshrefi, S.M., Ahmed, R.T. (2019). One step to synthesis (rGO/Ni NPs) nanocomposite and using to adsorption dyes from aqueous solution. Materials Today: Proceedings, 19: 94-101. https://doi.org/10.1016/j.matpr.2019.07.663